Modelling roll waves with shallow water equations and turbulent closure

ZHIXIAN CAO, Professor, [a]*State Key Laboratory of Water Resources and Hydropower Engineering Science, Wuhan University, China;* and Professor, [b]*Institute for Infrastructure and Environment, Heriot-Watt University, UK*

Email: zxcao@whu.edu.cn (author for correspondence)

PENGHUI HU, PhD student, *State Key Laboratory of Water Resources and Hydropower Engineering Science, Wuhan University, China*

Email: 2008301580223@whu.edu.cn

KAIHENG HU, Professor, *Institute of Mountain Hazards and Environment, Chinese Academy of Sciences, China*

E-mail: khhu@imde.ac.cn

GARETH PENDER (IAHR Member), Professor, [a]*Institute for Infrastructure and Environment, Heriot-Watt University, UK;* Visiting Professor, [b]*State Key Laboratory of Water Resources and Hydropower Engineering Science, Wuhan University, China*

Email: g.pender@hw.ac.uk

QINGQUAN LIU, Professor, *Institute of Mechanics, Chinese Academy of Sciences, China*

Email: qqliu@imech.ac.cn

ABSTRACT

A physically enhanced model is proposed for roll waves based on the shallow water equations and $k-\varepsilon$ turbulence closure along with a modification component. It is tested against measured data on periodic permanent roll waves, and the impact of turbulence is demonstrated to be essential. It is revealed that a regular inlet perturbation may lead to periodic permanent or natural roll waves, when its period is shorter or longer than a critical value inherent to a specified normal flow. While a larger amplitude or shorter period of a regular inlet perturbation is conducive to the formation of periodic permanent roll waves, their period remains the same as that of the perturbation, while their amplitude increases with the perturbation period and is independent of the perturbation amplitude. An irregular inlet perturbation favours the formation of natural roll waves, so does a larger amplitude of the perturbation.

Keywords: $k-\varepsilon$ turbulence model; natural roll waves; periodic permanent roll waves; shallow water equations; turbulent Reynolds stress

1. Introduction

Roll waves are successive hydraulic bores that usually occur in shallow flows down an inclined slope (Dressler 1949, Brock 1967, Balmforth and Mander 2004). Although roll waves can develop on laminar fluid films and non-Newtonian fluids (Benjamin 1957, Yih 1963, Liu and Mei 1994, Tamburrino and Ihle 2013), the present work focuses on roll waves of clear water in the turbulent regime. Generally, roll waves are undesirable for man-made conduits because they can trigger excessive intermittent pressures and stresses (Dressler 1949). Moreover, roll waves are ubiquitous in debris flows, and substantially contribute to their destructive power and affect the deposition of debris (Zanuttigh and Lamberti 2007, Iverson *et al*. 2010). Therefore roll waves are of practical significance, and merit systematic investigations.

Since the first observation by Cornish (1934), numerous investigations have been carried out to enhance the understanding of roll wave dynamics, including analytical research, laboratory experiment and mathematical modelling. Experimental studies of roll waves are rare, and only Brock (1967) conducted systematic experiments in laboratory flumes. This work comprised two kinds of experiments: the first concerned roll wave trains that develop naturally in a uniform flow, whilst the second reproduced periodic permanent roll waves to compare with theoretical analyses. To accelerate the formation of roll waves in a finite length, small disturbances (perturbations) were imposed at the flume inlet. Such small disturbances increased downstream and developed into roll waves. For periodic permanent roll waves, the apparatus at the inlet of the channel was set to oscillate at the desired period. However, the perturbation characteristics for natural roll waves were not described by Brock (1967).

To date, mathematical modelling of roll waves is far from mature and few mathematical models have been used to model roll waves (Zanuttigh and Lamberti 2002), while there have been a number of analytical investigations (Jeffreys 1925, Dressler 1949, Dressler and Pohle 1953, Iwasa 1954, Needham and Merkin 1984, Kranenburg 1992, Yu and Kevorkian 1992, Balmforth and Mander 2004, Liu *et al.* 2005, Richard and Gavrilyuk 2012). Most of these investigations are based on traditional shallow water equations - SWEs (Jeffreys 1925, Dressler 1949, Dressler and Pohle 1953, Zanuttigh and Lamberti 2002, Liu *et al.* 2005), in which turbulent Reynolds stress is almost exclusively ignored without justification, except the rather simplistic estimation with a constant-viscosity (Needham and

Merkin 1984, Kranenburg 1992, Balmforth and Mander 2004). Arguably this was motivated by the fact that turbulent Reynolds stress is generally negligible in fluvial flows over mild beds. However, roll waves advancing downstream can be intensely turbulent (Cornish 1934, Dressler 1949), and large-scale vortexes arise behind the shocks (Richard and Gavrilyuk 2012). Theoretical analyses (Jeffreys 1925, Stoker 1958) show that perturbations to the uniform flow would grow and result in roll waves over steep slopes if the Froude number $\mathrm{F} = U/\sqrt{gh\cos\theta} > 2$ (where h is the flow depth in the normal direction of slope; U is the depth-averaged streamwise velocity; θ is the angle of the bed slope; and g is the gravitational acceleration). Other analyses indicate that the critical Froude number for roll wave formation depends on the channel shape, friction law and velocity distribution (Dressler and Pohle 1953, Iwasa 1954) and varies around 2. Dressler (1949) constructed a periodic discontinuous solution to describe stationary roll waves. However, serious discrepancies exist between Dressler's solution and Brock's (1967) experiments, especially for steep slopes (Brock 1970). Dressler's theory presents a zero thickness across the shocks while the thickness is demonstrated to be finite in experiments. Besides, the wave amplitude from Dressler's theory largely exceeds the measured data. Zanuttigh and Lamberti (2002) numerically modelled the evolution of natural roll waves using traditional SWEs with the weighted-average-flux (WAF) method (Toro 2001). They conducted comparisons with experimental data from Brock (1967) on bore height and average wave period. Regretfully, the model by Zanuttigh and Lamberti (2002) was not evaluated against the very detailed observed data of the wave profile of periodic permanent roll waves (Brock 1967), and accordingly the modelling study of natural roll waves is open to question. Based on Dressler's (1949) and Brock's (1970) work, Liu *et al.* (2005) developed an analytical treatment for roll wave dynamics, focusing on the influence of shear stress on soil erosion. To further investigate roll wave dynamics, Needham and Merkin (1984) attempted to introduce a constant turbulent viscosity into the SWE model. Unfortunately, such a simplification fails to improve the results accurately (Yu and Kevorkian 1992). Recently, the Richard–Gavrilyuk equations (RGE) were proposed to study roll waves (Richard and Gavrilyuk 2012), in which two types of enstrophies are incorporated to represent the dispersion due to the non-uniform velocity distribution in the vertical. One was a small-scale enstrophy φ generated near the bed, and the other was a large-scale enstrophy Φ associated with roller eddies in the hydraulic jumps. The solutions of the RGE model were in reasonable agreement with the experimental

profiles of periodic permanent roll waves measured in Brock's (1967) experiments. However, the RGE model hinges upon the prior specifying of the flow depth and velocity at a critical point (Richard and Gavrilyuk 2012, subsection 3.3). In the evaluation of the RGE model, the observed data from Brock's experiment was used to specify the flow depth and velocity at the critical point. But for cases without observed data, the RGE model does not work at all. The RGE model is able to resolve sufficiently developed, stationary roll waves only, but not the formation processes of roll waves. Moreover, the dispersion that accounts for the vertical non-uniformity of velocity is confused with turbulence in the RGE model. It is important to note that the dispersion has nothing to do with turbulence (Rodi 1993).

The present paper presents a physically enhanced SWE model incorporating the impacts of turbulent Reynolds stress (SWE-TM). The standard depth-averaged $k-\varepsilon$ turbulence model proposed by Rastogi and Rodi (1978) is introduced to determine the Reynolds stress along with a modification component. To solve the governing equations an operator-splitting framework is applied. For the hyperbolic system, a second-order accurate Godunov-type finite volume method is used along with the HLLC (Harten-Lax–van Leer Contact Wave) approximate Riemann solver for the homogeneous equations (Toro 2001). The nonhomogeneous parabolic equations are solved using an implicit discretization with the double-sweep method. The SWE-TM model is tested against Brock's (1967) experimental data on periodic permanent roll waves. It is compared with typical existing SWE models, including: (a) a traditional SWE model without accounting for either turbulence closure or dispersion; (b) a SWE model incorporating the standard depth-averaged $k-\varepsilon$ turbulent closure (SWE-T); (c) a SWE model incorporating the standard depth-averaged $k-\varepsilon$ turbulent closure and dispersion (SWE-TD); and (d) the RGE model due to Richard and Gavrilyuk (2012). Then the present SWE-TM model is deployed to investigate the formation process and evolution of both periodic permanent roll waves and natural roll waves, and the impacts of the perturbations imposed at the channel inlet are evaluated.

2. Mathematical equations

2.1 *Governing equations*

It is justified to employ the shallow water equations in roll waves modelling even though they are

based on the assumption of hydrostatic pressure, because the impact of this assumption is small relative to the other physical influences in rapidly varied flow such as hydraulic jumps (Gharangik and Chaudhry 1991). The general 1D shallow water equations comprise the mass and momentum conservation equations over arbitrary slopes. As turbulence Reynolds stress and dispersion are incorporated, these equations read

$$\frac{\partial h}{\partial t}+\frac{\partial (hU)}{\partial x}=0 \tag{1}$$

$$\frac{\partial hU}{\partial t}+\frac{\partial}{\partial x}\left(hU^2+\frac{1}{2}g'h^2\right)=gh\sin\theta+\frac{\partial hT_R}{\partial x}-\frac{\partial D}{\partial x}-\frac{\tau_b}{\rho} \tag{2}$$

where t is time; x is the streamwise coordinate parallel to slope; $g'=g\cos\theta$; T_R is the depth-averaged Reynolds stress; D is the dispersion momentum transport; τ_b is the bed friction stress; and ρ is the density of water. On the right-hand side (RHS) of Eq. (2), the first (S_G) and second (S_{T_R}) terms indicate the effects of gravity and turbulent Reynolds stress respectively, while the third term (S_D) represents dispersion. In Eqs. (1) and (2), the effects of the bottom slope are fully incorporated (Savage and Hutter 1991, Bouchut *et al*. 2003), albeit often ignored in most shallow water flow models.

2.2 *Model closure*

To close the governing equations, auxiliary relationships and equations have to be introduced to determine the bed friction, dispersion and Reynolds stress. The bed friction stress τ_b is estimated by

$$\tau_b=\rho C_f U|U| \tag{3}$$

where C_f is the friction coefficient. The dispersion momentum transport D accounts for the effect of vertical non-uniform distribution of velocity, which is defined as follows

$$D=\int_{z_0}^{z_0+h}\left[\bar{u}(z)-U\right]^2\mathrm{d}z=\beta\, hU^2, \qquad \beta=\frac{1}{h}\int_{z_0}^{z_0+h}\left[\bar{u}(z)/U-1\right]^2\mathrm{d}z \tag{4a, b}$$

where $\bar{u}(z)$ is the streamwise velocity distribution in vertical; z_0 is the zero velocity level; β is the momentum flux correction (Kranenburg 1992, Zanuttigh and Lamberti 2007), which can be evaluated when the velocity distribution is specified. Although the flow structure of the weak hydraulic jump was studied experimentally (Misra *et al.* 2008), the velocity distribution in roll wave remains poorly understood. Based on a power law distribution and log law distribution for the

streamwise velocity (Iwasa 1954, Jin and Steffler 1993, Duan and Nanda 2006, Wu 2007), one can readily derive

$$\beta_{power} = \frac{1}{m(m+2)} \tag{5a}$$

$$\beta_{log} = \frac{-\eta_0 \ln\eta_0(\ln\eta_0 - 2) + 2\eta_0(1-\eta_0)(1-\ln\eta_0) - (\eta_0 - 1)^3}{(\eta_0 - 1 - \ln\eta_0)^2} \tag{5b}$$

where m is typically around 7; and $\eta_0 = z_0 / h$ is the dimensionless zero bed elevation. Equations (5a, b) represent the momentum flux correction in relation to the power law and log law distribution respectively. According to Brock (1967), the value of β is about 0.02 for a smooth channel and 0.05 for a rough channel, which agree with Eqs. (5a, b).

In a traditional turbulence closure model, the depth-averaged Reynolds stress T_R is determined following Boussinesq's eddy-viscosity concept (Rastogi and Rodi 1978)

$$T_R = T_0 = 2\nu_t \frac{\partial U}{\partial x} - \frac{2}{3}k \tag{6}$$

where k is the depth-averaged turbulent kinetic energy; $\nu_t = C_\mu k^2 / \varepsilon$ is the depth-averaged eddy viscosity; ε is the depth-averaged turbulent dissipation rate; and C_μ is an empirical coefficient. Here the standard depth–averaged $k-\varepsilon$ turbulence model due to Rastogi and Rodi (1978) is used

$$\frac{\partial(hk)}{\partial t} + \frac{\partial(hUk)}{\partial x} = \frac{\partial}{\partial x}\left(\frac{\nu_t}{\sigma_k} h \frac{\partial k}{\partial x}\right) + hP_k + hP_{kb} - \varepsilon h \tag{7}$$

$$\frac{\partial(h\varepsilon)}{\partial t} + \frac{\partial(hU\varepsilon)}{\partial x} = \frac{\partial}{\partial x}\left(\frac{\nu_t}{\sigma_\varepsilon} h \frac{\partial \varepsilon}{\partial x}\right) + h\frac{\varepsilon}{k}\left(C_{\varepsilon 1} P_k - C_{\varepsilon 2}\varepsilon\right) + hP_{\varepsilon b} \tag{8}$$

where P_k is the production of turbulence due to the horizontal velocity gradients, defined as $P_k = 2\nu_t (\partial U / \partial x)^2$; P_{kb} and $P_{\varepsilon b}$ are the production terms from non-uniformity of vertical profiles, related to the friction velocity u_* by $P_{kb} = C_f^{-1/2} u_*^3 / h$ and $P_{\varepsilon b} = C_\Gamma C_{\varepsilon 2} C_\mu^{1/2} C_f^{-3/4} u_*^4 / h^2$ (Rastogi and Rodi 1978), where $u_* = \sqrt{\tau_b / \rho}$. The values of the relevant coefficients are listed in Table 1 (Launder and Spalding 1974).

Table 1 Coefficients in the standard depth–averaged $k-\varepsilon$ turbulence model

C_μ	$C_{\varepsilon 1}$	$C_{\varepsilon 2}$	σ_k	σ_ε	C_Γ
0.09	1.44	1.92	1.0	1.3	3.6

It is recognized that the standard $k-\varepsilon$ turbulence closure model is valid for fully developed, high-Reynolds-number turbulent flows (Rodi 1993), but the turbulence in roll waves over steep slopes may not be fully developed. For example, in Brock's (1967) experiments, the value of the Reynolds number $\mathrm{Re}=rU/\nu$ is typically of the order of 1.0E3 at the trough of the roll waves, where r is the hydraulic radius and the water viscosity ν =1.0E-6 m^2 s^{-1}. Equally importantly, errors may arise from the depth-averaging process of the $k-\varepsilon$ model, this is critical as the flow structure along the flow depth varies dramatically in roll waves. It follows that a modification component to the standard depth-averaged $k-\varepsilon$ closure for turbulence is warranted, which is shown to be necessary below for the test cases related to the experiments by Brock (1967). Ni (2010) proposed the following Reynolds stress-like relationship,

$$T_a = 2\alpha h u_* \frac{\partial U}{\partial x} \tag{9}$$

where α is an empirical coefficient to be calibrated using observed data. It is referred to as dispersion by Ni (2010), which however is not justified. The dispersion momentum transport D is always non-negative according to the definition Eqs. (4a, b), yet it could be either positive or negative if modelled by Eq. (9). In this connection, the approximation [i.e., Eq. (2.4)] to the integration of momentum flux by Kranenburg (1992) is open to question. It follows that Eq. (9) should rather be regarded as an empirical modification to the turbulent Reynolds stress in Eq. (6). Accordingly,

$$T_R = T_0 + T_a \tag{10}$$

The modification in turbulent stress is evaluated below for specific cases of roll waves.

Briefly, in a traditional SWE model, $T_R = D = 0$. In the SWE-T model, $T_R = T_0$ by Eq. (6) and $D=0$. In the SWE-TD model, $T_R = T_0$ by Eq. (6) and D by Eq. (4), and in the SWE-TM model, $T_R = T_0 + T_a$ by Eq. (10) and $D=0$.

2.3 *Numerical scheme*

Equations (1), (2), (7) and (8) constitute a fourth-order system, and can be written in a conservative

form as follows

$$\frac{\partial \boldsymbol{U}}{\partial t}+\frac{\partial \boldsymbol{F}}{\partial x}=\boldsymbol{S} \tag{11}$$

$$\boldsymbol{U}=\begin{bmatrix} h \\ q \\ hk \\ h\varepsilon \end{bmatrix}=\begin{bmatrix} h \\ hU \\ hk \\ h\varepsilon \end{bmatrix},\quad \boldsymbol{F}=\begin{bmatrix} hU \\ hU^2+\frac{1}{2}g'h^2 \\ hUk \\ hU\varepsilon \end{bmatrix} \tag{12a, b}$$

$$\boldsymbol{S}=\boldsymbol{S}_s+\boldsymbol{S}_f+\boldsymbol{S}_d=\begin{bmatrix} 0 \\ gh\sin\theta \\ 0 \\ 0 \end{bmatrix}+\begin{bmatrix} 0 \\ -\frac{\tau_b}{\rho} \\ hP_k+hP_{kb}-\varepsilon h \\ h\frac{\varepsilon}{k}\left(C_{\varepsilon 1}P_k-C_{\varepsilon 2}\varepsilon\right)+hP_{\varepsilon b} \end{bmatrix}+\begin{bmatrix} 0 \\ \frac{\partial hT_R}{\partial x}-\frac{\partial D}{\partial x} \\ \frac{\partial}{\partial x}\left(\frac{\nu_t}{\sigma_k}h\frac{\partial k}{\partial x}\right) \\ \frac{\partial}{\partial x}\left(\frac{\nu_t}{\sigma_\varepsilon}h\frac{\partial \varepsilon}{\partial x}\right) \end{bmatrix} \tag{12c}$$

where $\boldsymbol{T}$ represents the conservative variables; $\boldsymbol{U}$ is the flux variables; $\boldsymbol{S}$ is the RHS term comprising the gravitational term in $\boldsymbol{S}_s$, the friction and the source terms of the $k-\varepsilon$ model in $\boldsymbol{S}_f$, and also the turbulent Reynolds stress and dispersion as well as the diffusion terms of the $k-\varepsilon$ model in $\boldsymbol{S}_d$.

An operator-splitting algorithm is introduced to solve Eq. (11). In the first sub-step, the hyperbolic operator is dealt with,

$$\boldsymbol{U}_i^p=\boldsymbol{U}_i^j-\Delta t\left(\boldsymbol{F}_{i+1/2}-\boldsymbol{F}_{i-1/2}\right)^j/\Delta x \tag{13}$$

where Δt is the time step; Δx is the spatial step; i is the spatial node index; j is the time step index; p represents the state updated from Eq. (13); and $\boldsymbol{F}_{i+1/2}$ and $\boldsymbol{F}_{i-1/2}$ are the interface fluxes computed using the HLLC Riemann solver (Toro 2001). The MUSCL method is employed to achieve the second-order accuracy in space for the Riemann state reconstruction. Here the variables k and ε are passive scalars and solved as the third component (contact wave) in the HLLC solver (Toro 2001), similar to the solution of sediment concentration in a coupled shallow water hydrodynamic and sediment transport model (Cao *et al*. 2004).

Following Eq. (13), a second sub-step is necessary to update the conservative variables ($h, q, hk, h\varepsilon$) to a new time step. This involves the solution of a non-homogeneous parabolic system comprising the RHS term in Eq. (11). An implicit discretization of the dispersion and diffusion terms is implemented for stability. To take advantage of the double-sweep method for the resulting algebraic equations, linearization is introduced where necessary. Thus,

$$\boldsymbol{U}_i^{j+1} = \boldsymbol{U}_i^{p} + \Delta t\left(\boldsymbol{S}_s + \boldsymbol{S}_f\right)_i^{p} + \Delta t\boldsymbol{S}_{di}^{j+1} \tag{14}$$

In Eq. (14), the second-order terms in $\boldsymbol{S}_{di}^{j+1}$ are discretized as

$$\frac{\partial}{\partial x}\left(C\frac{\partial \phi}{\partial x}\right)\Bigg|_i^{j+1} = \frac{1}{\Delta x}\left[C_{i+1/2}^{p}\left(\frac{\partial \phi}{\partial x}\right)\Bigg|_{i+1/2}^{j+1} - C_{i-1/2}^{p}\left(\frac{\partial \phi}{\partial x}\right)\Bigg|_{i-1/2}^{j+1}\right] \tag{15}$$

where ϕ is a general variable representing U, k or ε, and C indicates the coefficient in line with ϕ. The inter-cell values $C_{i+1/2}^{p} = (C_{i+1}^{p} + C_i^{p})/2$ and $C_{i-1/2}^{p} = (C_i^{p} + C_{i-1}^{p})/2$ are the linearized coefficients, and $(\partial\phi/\partial x)_{i+1/2}^{j+1} = (\phi_{i+1}^{j+1} - \phi_i^{j+1})/\Delta x$, $(\partial\phi/\partial x)_{i-1/2}^{j+1} = (\phi_i^{j+1} - \phi_{i-1}^{j+1})/\Delta x$.

Further, the first-order terms in $\boldsymbol{S}_{di}^{j+1}$ relate to dispersion (if $\beta \neq 0.0$) and k. Both terms are discretized with a linearization of the velocity and flow depth as necessary, i.e.,

$$\frac{\partial D}{\partial x}\Bigg|_i^{j+1} = \frac{\partial}{\partial x}\left(\beta\, hU^2\right)\Bigg|_i^{j+1} = \frac{1}{2\Delta x}\left[\left(\beta\, hU\right)_{i+1}^{p} U_{i+1}^{j+1} - \left(\beta\, hU\right)_{i-1}^{p} U_{i-1}^{j+1}\right] \tag{16a}$$

$$\frac{\partial}{\partial x}\left(\frac{2hk}{3}\right)\Bigg|_i^{j+1} = \frac{1}{3\Delta x}\left[h_{i+1}^{p} k_{i+1}^{j+1} - h_{i-1}^{p} k_{i-1}^{j+1}\right] \tag{16b}$$

Indeed, the two terms discretized in Eq. (16a, b) are purely functions of the state variables. Theoretically, it would be natural to place both terms in the left-hand-side (LHS) of Eq. (2) for solution. However, this will make the well-established HLLC Riemann solver (Toro 2001) not directly applicable for the hyperbolic part of the equations. The present work aims to keep the LHS of the equations the same as that of the traditional SWEs, while all the "extra" terms involved in the Reynolds stress and dispersion are put on the RHS for easier modelling. This idea is in principle quite similar to that implemented in the recent work on a double-layer averaged model (Li *et al*. 2013).

The numerical scheme for the homogeneous hyperbolic system is explicit and stability is controlled by the Courant number

$$Cr = \frac{\left(U \pm \sqrt{g'h}\right)_{max} \Delta t}{\Delta x} \le 1 \tag{17}$$

3. Case study - periodic permanent roll waves

Brock (1967) conducted experiments on two types of roll waves in laboratory flumes, as briefed above. The experimental observations on periodic permanent roll wave are employed to test the models in this section. Two flumes were used by Brock (1967) to produce periodic permanent roll waves. One was 36.6 m long with slopes of 0.0502 and 0.0846, and the other was 24.4 m long with a slope of 0.12. The widths of both flumes were 11.75 cm. In this section, numerical simulations are conducted using the same conditions as in Brock's (1967) experiments (summarized in Table 2). The initial water depth is 0.0 m. The amplitude of the perturbations imposed at the inlet of the channel is equal to 0.5% of the normal flow depth following Zanuttigh and Lamberti (2002). A steady water discharge Q is fed at the inlet and the water depth is set as

$$h_{in} = h_n + h_{am}\sin\left(2\pi t / T\right) \tag{18}$$

where T is the perturbation period imposed at the inlet of the channel; h_n is the normal depth; and the perturbation amplitude $h_{am} = 0.5\% h_n$. The Froude number $\mathrm{F_n}$ at the inlet of the channel refers to the normal conditions. In Table 2, l_p indicates the distance required for the perturbations to fully develop into periodic permanent roll waves, as computed by the SWE-TM model. We set the computational reach long enough to ensure that the forward wave does not reach the downstream boundary within the time of computation, thus the downstream boundary condition can be simply set at the initial static state. A dimensionless water depth h^* is defined as $h^* = h/h_n$. For all the cases in the present work, the spatial step is set to be 0.001 m to achieve grid independence, and the Courant number is 0.5.

To quantify the difference between numerical solutions and measured data, the dimensionless discrepancy is defined with the L^1-norm

$$L^1 = \frac{\sum abs\left(\hat{h} - h^*\right)}{\sum \hat{h}} \tag{19}$$

where $\hat{h}$ is dimensionless measured water depth scaled with h_n.

Table 2 Summary of experimental cases about periodic permanent roll waves

Case	$\tan\theta$	Q ($m^3 s^{-1}$)	h_n (mm)	F_n	C_f	T (s)	l_p (m)
1	0.0502	9.72×10^{-4}	7.98	3.71	0.0032	1.218	32.3
2						0.934	29.0
3	0.0846	6.52×10^{-4}	5.28	4.63	0.0036	1.12	21.7
4						0.796	17.3
5	0.1201	8.02×10^{-4}	5.33	5.6	0.0035	0.695	16.3
6						1.015	21.1

3.1 *Performances of the SWE, SWE-T and SWE-TD models*

The SWE, SWE-T and SWE-TD models are assessed by comparison with measured data for Case 5 (Table 2). The dispersion term in the SWE-TD model is simulated based on the momentum flux correction β in Eq. (5). Figure 1 shows the dimensionless water depth in a single permanent roll wave computed from the SWE, SWE-T and SWE-TD models, along with the measured data from Brock (1967), where λ is the wavelength. Apparently the SWE model performs poorly compared to measurements. Though the SWE-T model features improved performance over the SWE model, the deviations are still considerable from the measured data, characterizing that it is insufficient to accurately resolve the wave profile by incorporating the impact of turbulent Reynolds stress based on the standard depth-averaged $k-\varepsilon$ model. One might argue that dispersion may play a considerable role. However, the computed flow depth around the wave crest from the SWE-TD model decreases excessively without any improvement in the crest location. The model performance gets even worse after incorporating turbulent Reynolds stress and dispersion simultaneously. Even if β is tuned by multiplying a factor from 0.05 to 0.8 to reflect the uncertainty arising from the assumed power or logarithmic distribution of the mean velocity, the solutions cannot be improved (not shown). It follows that including dispersion is not a viable way to improve the modelling of permanent roll waves, echoing the suggestion by Kranenburg (1992). Rather, it is suggested that a modification to the Reynolds stress based on the standard depth-averaged $k-\varepsilon$ turbulent model is implemented, which

is essentially the SWE-TM model as calibrated and assessed below using the experimental data of Brock (1967).

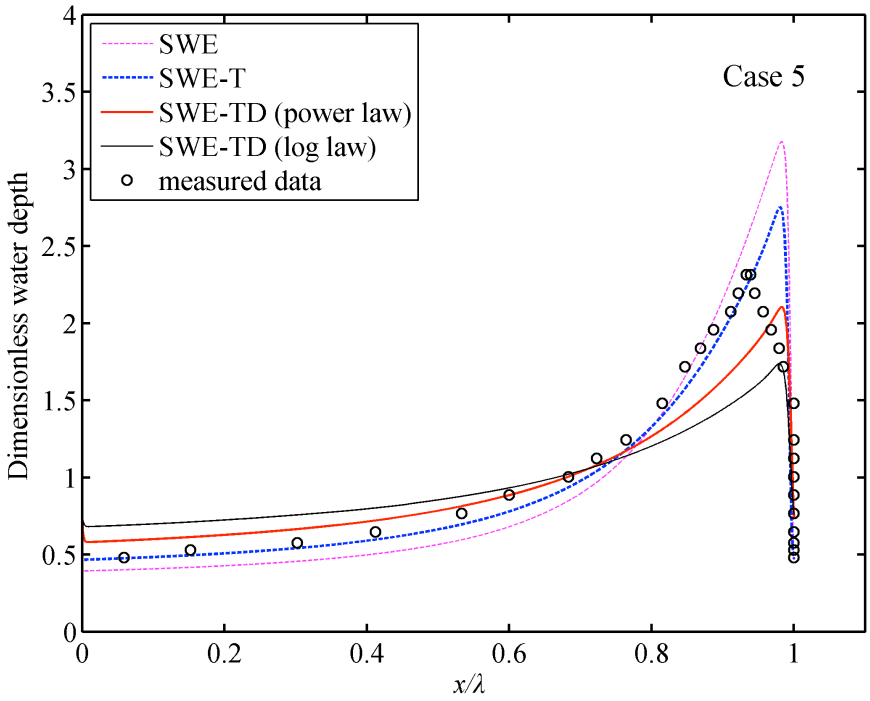

Figure 1 Comparison between the computed water depth from the SWE, SWE-T and SWE-TD models and measured data from Brock (1967)

3.2 *Performance of the SWE-TM model*

3.2.1 *Calibration for* α

The empirical coefficient α in Eq. (9) should be calibrated under different conditions. As the Froude number is in general the critical factor in roll wave formation (Jeffreys 1925, Stoker 1958), it is appropriate to relate the coefficient α to the Froude number F_n (Table 2) imposed at the inlet of the channel from normal conditions. The value of critical Froude number is 2.0 for a rectangular channel with an unvarying friction coefficient (Brock 1967) and α is set to be 0.0 if $F \le 2.0$. The parameters in the standard depth-averaged $k-\varepsilon$ model are kept unchanged (Table 1). The coefficient α is calibrated for Case 1, Case 3 and Case 5 as listed in Table 3, based on the minimization of the

L^1-norm. A fitting relationship between α and the Froude number F_n can be readily derived,

$$\alpha = \begin{cases} 0.1867F_n^2 + 0.5096F_n - 1.766 & \text{if } F_n > 2.0 \\ 0.0 & \text{if } F_n \le 2.0 \end{cases} \tag{20}$$

Figure 2 shows the comparisons between the computed water depth of a single permanent wave by the SWE-TM model and measured data of Brock (1967) using the calibrated values of α. The water depth increases gradually from the trough to the crest, and then drops sharply to the minimum. The solutions of SWE-TM model agree well with measured data, not only in the water depth but also in the location of wave crest. The improvement is obviously substantial compared to those models shown in Fig. 1.

Table 3 Calibrated values of α

F_n	α
≤ 2.0	0.0
3.71	2.8
4.63	4.5
5.6	7.0

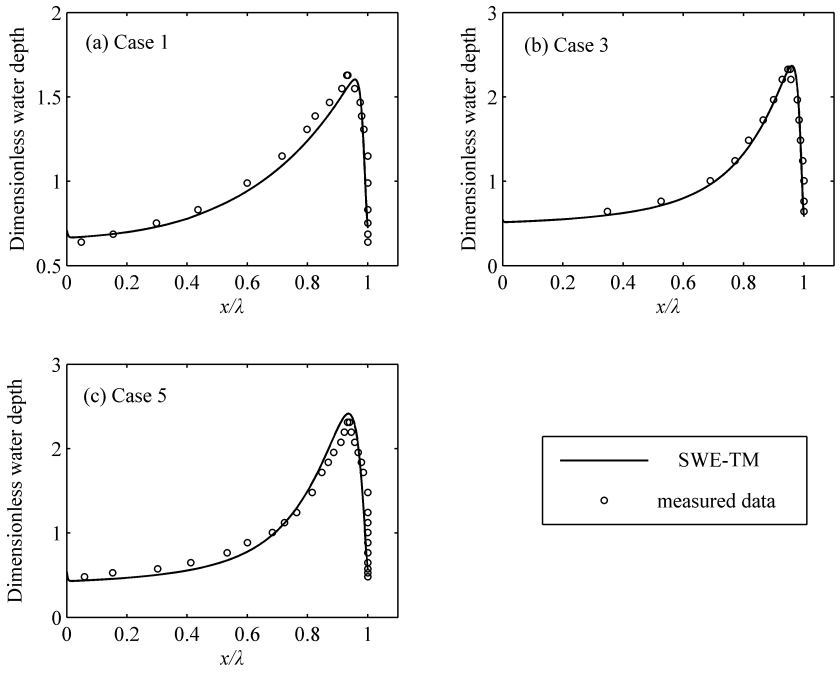

Figure 2 Comparison between the computed water depth from the SWE-TM model using calibrated

α and measured data from Brock (1967)

3.2.2 *Impacts of coefficients in* $k-\varepsilon$ *turbulence model*

It is interesting to find out how the coefficients in $k-\varepsilon$ turbulence model affect the results of the SWE-TM model using the calibrated α. Indeed, the dissipation rate ε is dictated by small-scale eddies and to date remains one of the fundamental quantities that could not be modelled accurately in the context of turbulence modelling. Thus uncertainty is inevitable in modelling the ε equation (Shi 1994). Moreover, Rastogi and Rodi (1978) pointed out that the $k-\varepsilon$ model in the depth-averaged version is simplified and empirical, and sensitive to the coefficients. From our numerical tests, the results are more sensitive to the coefficient C_{Γ} than the others (not shown). Therefore, C_{Γ} is tuned to demonstrate its impact on roll waves within the SWE-TM model.

Specifically, the value of C_{Γ} is tuned for Case 1 (Table 4). The corresponding values of the L^1-norm are listed in Table 4, which show that an increased value of C_{Γ} (=4.5) results in improved agreement with the observed data, as indicated by the reduced value of L^1-norm. This is also seen in Fig. 3 that shows the computed water depth in comparison with the measured data. Nevertheless, for Case 3 and Case 5 (results not shown), the most favorable value of C_{Γ} is still 3.6 in the standard depth-averaged $k-\varepsilon$ model (Table 1). Therefore Case 1 is a special case, which requires a tuned value of C_{Γ} for agreement with observed data within the SWE-TM model.

Table 4 Values of L^1-norm in relation to different values of C_{Γ} for Case 1

C_{Γ}	Case 1		
	2.2	3.6	4.5
L^1-norm (%)	6.68	5.82	5.33

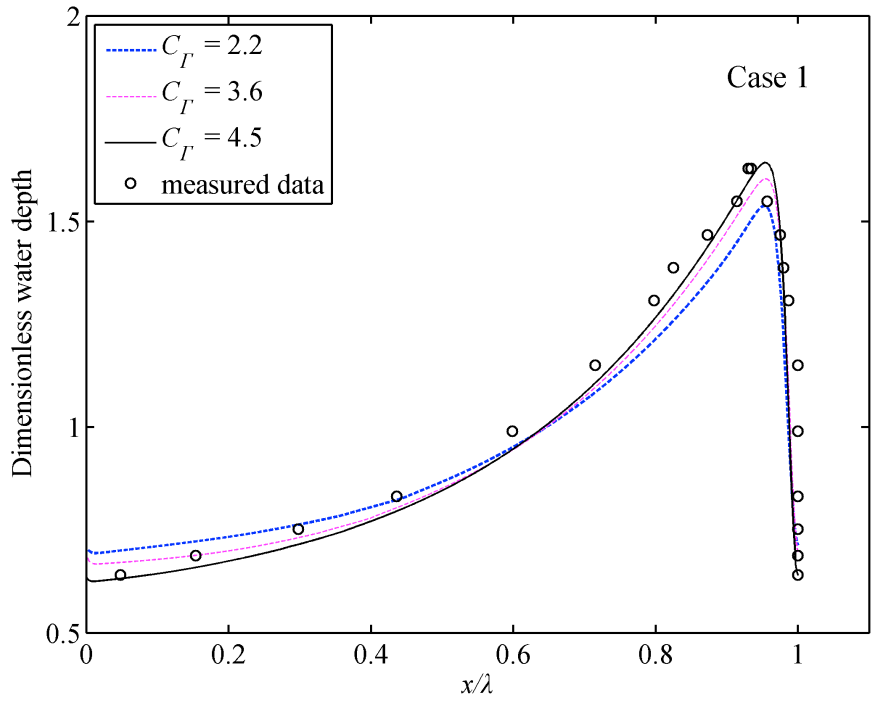

Figure 3 Comparison between the computed water depth from SWE-TM model using tuned C_Γ for Case 1 and measured data from Brock (1967)

3.3 *Model verification*

To verify the SWE-TM model, other cases in Brock's (1967) experiments are studied with the calibrated relationship Eq. (20) for α and the standard depth-averaged $k-\varepsilon$ model (Table 1). The SWE-TM model is also compared with the SWE, SWE-T and RGE model for Case 2, Case 4 and Case 6.

Figure 4 illustrates the water depth in a single permanent roll wave computed from the SWE, SWE-T, SWE-TM and RGE models along with the measured data. There are considerable discrepancies between the measurements and computed results from SWE and SWE-T models in water depth and location of the wave crest. Most notably, the SWE-TM model performs the best. Echoing Fig. 4, the values of the L^1-norm in Table 5 show improved performance of the present SWE-TM model over the RGE model of Richard and Gavrilyuk (2012) except for Case 2, which is in essence attributable to a single observed water depth (to the immediate right-hand-side of the observed crest) that apparently deviates from the overall trend characterized by the other observed water depths.

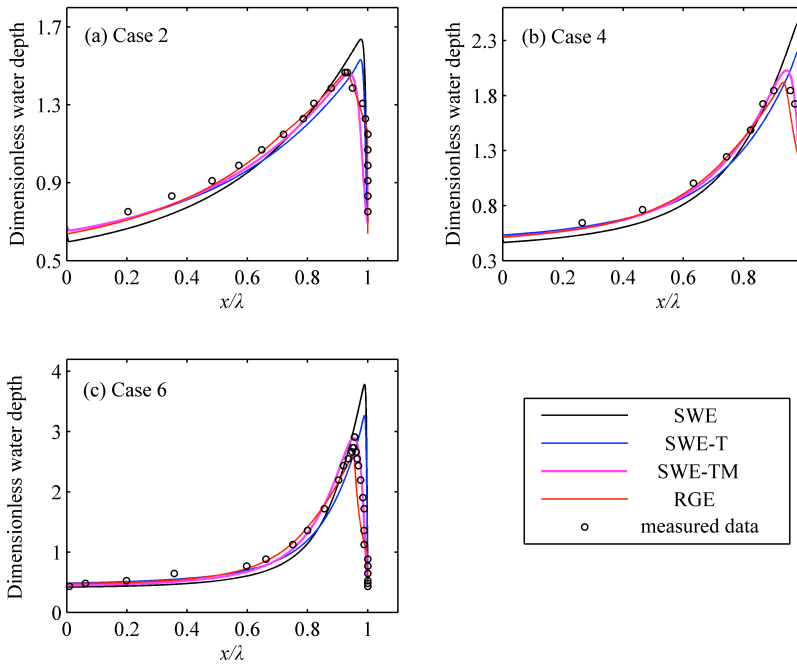

Figure 4 Comparison between the computed water depth and measured data from Brock (1967)

Table 5 Values of L^1-norm of SWE-TM and RGE models

	Case 2	Case 4	Case 6
SWE-TM (%)	4.41	4.65	6.43
RGE (%)	2.32	6.97	12.52

3.4 *Significance of turbulent Reynolds stress*

It has been shown that inclusion of turbulent Reynolds stress in the SWE-TM model does lead to improved performance in modelling roll waves (Fig. 4). Physically, this is not surprising at all because the turbulent Reynolds stress term S_{T_R} $(=S_{T_0}+S_{T_a})$ in the momentum conservation Eq. (2) is by no means negligible compared with the gravitational term $S_G=gh\sin\theta$. In relation to Case 5 of the experiments by Brock (1967), which features the largest bed slope (Table 2), Figure 5 shows the distribution of S_G, S_{T_0} and S_{T_a} in a single permanent wave from the SWE-TM model, where

$S_{T_0} = \partial(hT_0)/\partial x$ and $S_{T_a} = \partial(hT_a)/\partial x$, physically representing the turbulent Reynolds stress based on the standard depth-averaged $k-\varepsilon$ model and the modification component respectively. Compared to the gravitational term S_G, the turbulent Reynolds stress terms S_{T_0} and S_{T_a} are negligible from the trough to the peak of the waves. However, both are considerable downstream the wave crest, where large vortexes arise (Richard and Gavrilyuk 2012). Physically, turbulent Reynolds stress is critical in shaping the wave crest. It is noted that in the profiles of S_{T_0} and S_{T_a}, a minor fluctuation is discernible around the roll wave crest, which arise because both the water depth and velocity see an inflection. It is also recognized that Fig. 5 is based on computational modelling calibrated using observed data of the water depth. Detailed measured data of the turbulent structure of roll waves is warranted to facilitate further enhanced understanding of the phenomenon.

Within the present SWE-TM model, the modification component is estimated empirically based on existing experimental data of Brock (1967). Thus the model is applicable within the range of the maximum bed slope in the Brock's experiments (Table 2). Applications to higher bed slopes warrant sufficient caution, and further experiments are certainly necessary for extending the model's applicability.

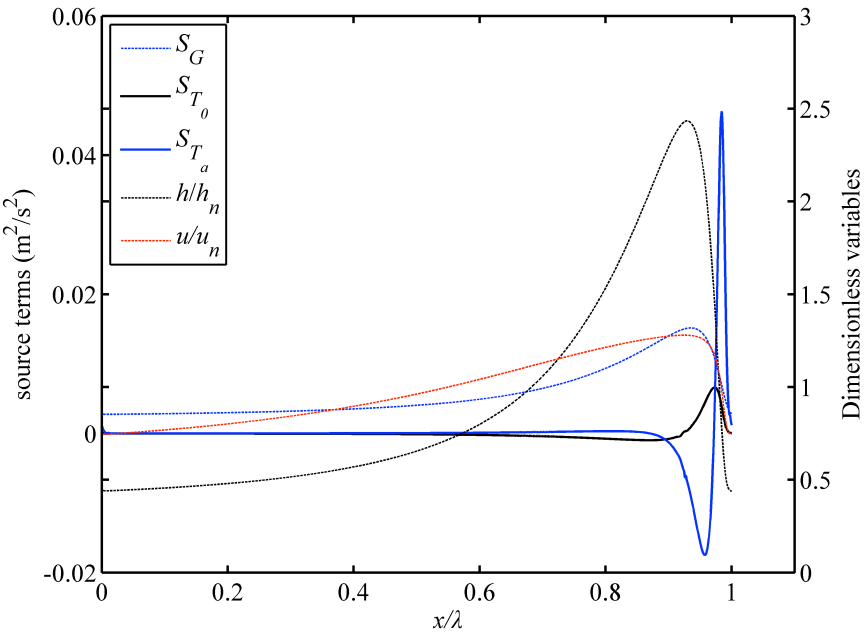

Figure 5 Computed Reynolds stress compared to the gravitational terms in a single permanent roll wave from the SWE-TM model

3.5 *Sensitivity analysis*

It is interesting to evaluate the sensitivity of the computed solutions of the SWE-TM model to coefficients α involved in the modification to Reynolds stress (Eq. 9) and C_T in the standard depth-averaged $k-\varepsilon$ turbulent closure model. Both coefficients are tuned by 30% based on the standard values from Eq. (20) and C_T=3.6 (Table 1). Here Case 2, Case 4 and Case 6 are considered.

Figure 6 shows the impacts of α on computed water depth from SWE-TM model. Qualitatively, α affects the roll wave profile in two ways, i.e., the value and location of the crest. In general, a larger α leads to a reduced peak water depth and moves the crest upstream, and vice versa. However, the changes are essentially negligible. Table 6 shows the values of the L^1-norm in relation to the tuned values of α, which suggests that the calibrated α as expressed by Eq. (20) are justified.

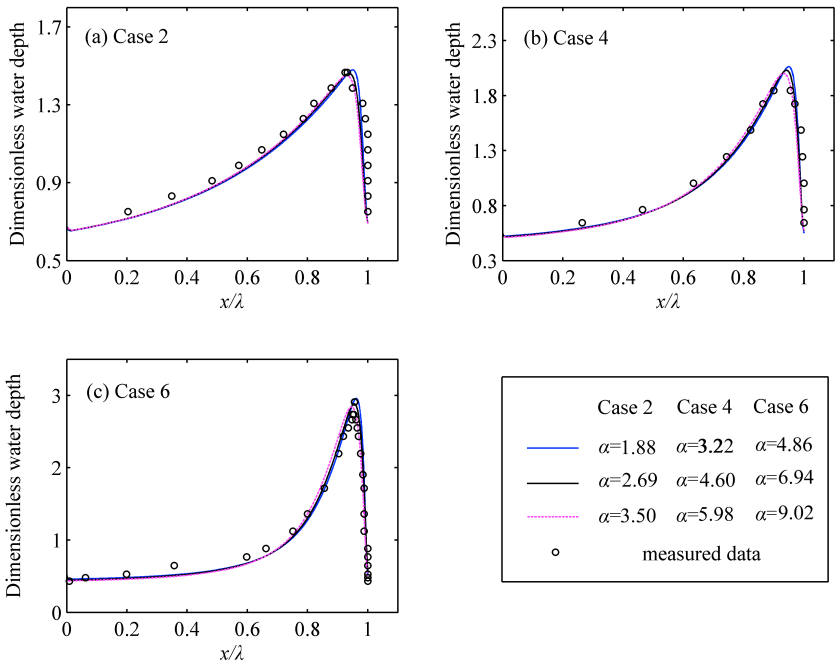

Figure 6 Impacts of α on water depth in SWE-TM model

Table 6 Values of L^1-norm in relation to different values of α

α	Case 2			Case 4			Case 6		
	1.88	2.69	3.50	3.22	4.60	5.98	4.86	6.94	9.02
L^1-norm (%)	4.54	4.41	4.52	5.92	4.65	4.89	6.86	6.43	6.95

The impacts of C_Γ on the computed water depth from the SWE-TM model are shown in Fig. 7 and Table 7. With the decrease of C_Γ, the impact of turbulence is enhanced and the peak water depth becomes smaller. However, C_Γ would not affect the location of the roll wave crest. For Case 4 and Case 6, C_Γ=3.6 is appropriate, while the value of C_Γ needs to be tuned larger for Case 2 (Table 7), which is once again attributable to a single observed water depth apparently deviating from the overall trend characterized by other observed water depths.

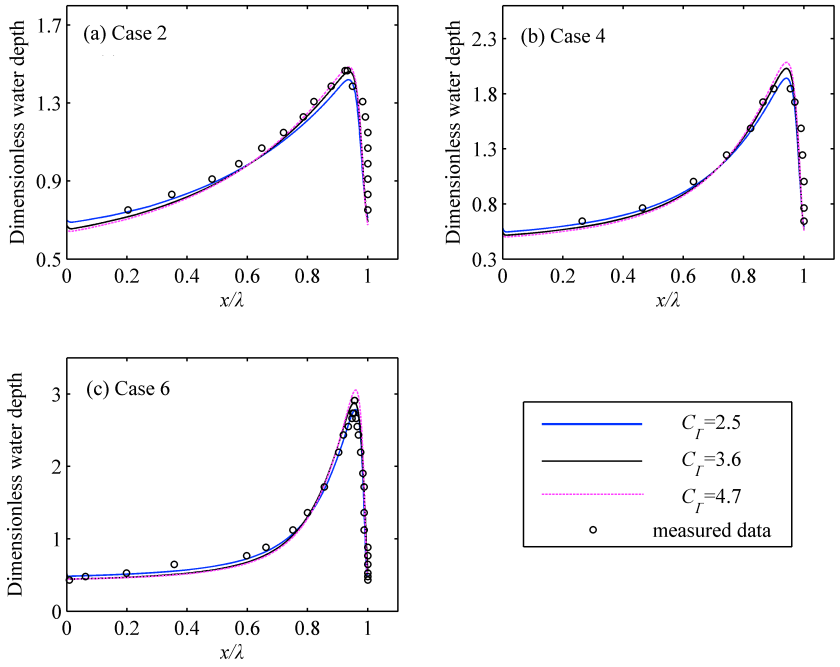

Figure 7 Impacts of C_Γ on water depth in SWE-TM model

Table 7 Values of L^1-norm in relation to different values of C_Γ

C_Γ	Case 2			Case 4			Case 6		
	2.5	3.6	4.7	2.5	3.6	4.7	2.5	3.6	4.7
L^1-norm (%)	5.04	4.41	4.14	4.99	4.65	5.71	7.67	6.43	8.39

3.6 *Formation process of periodic permanent roll waves*

Periodic permanent roll waves often generate from regular perturbations advancing a sufficiently long distance with a constant slope. Practically, however, the distance with a constant slope may not be long enough for perturbations to fully develop into periodic permanent roll waves, and as a result the perturbations evolve to premature roll waves. It is therefore interesting to understand the formation processes of period permanent roll waves.

The present SWE-TM model can be used to solve not only the fully developed, stationary roll waves (as shown above), but also the formation processes of roll waves. The present computational tests not only echo, but also extend the observations of Brock (1967). In contrast, the RGE model (Richard and Gavrilyuk 2012) cannot resolve the formation processes of roll waves, because it hinges upon a relationship at a critical point, which is prescribed using observed data.

Case 5 is considered as an example. Figure 8 illustrates the formation processes of periodic permanent roll waves computed from the SWE and SWE-TM models. Indeed, small regular perturbations at the inlet of the channel increase downstream and finally develop to periodic permanent roll waves, as described by Brock (1967). Also, as shown in Fig. 9, the wave profile remains the same at a given station and the wave properties do not change with stations after developing into a periodic permanent form (x=18 m, 26 m), which agrees well with Brock (1967). Equally importantly, the present computational tests indicate that the wave period is essentially the same as that of the perturbation imposed at the inlet during the formation and evolution of periodic permanent roll waves, which has not been specified by Brock (1967). Additionally, the wave amplitude of the SWE-TM model is smaller than that from the SWE model (Fig. 8), as a result of the turbulent Reynolds stress. The propagation speed and stationary wavelength are indistinguishable between these two models.

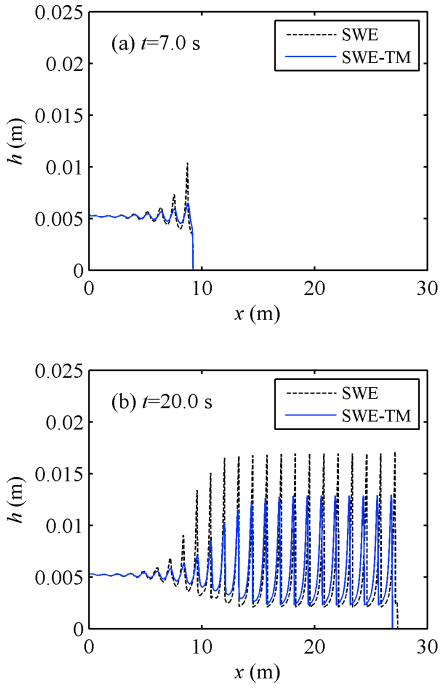

Figure 8 Formation process of periodic permanent roll waves in Case 5

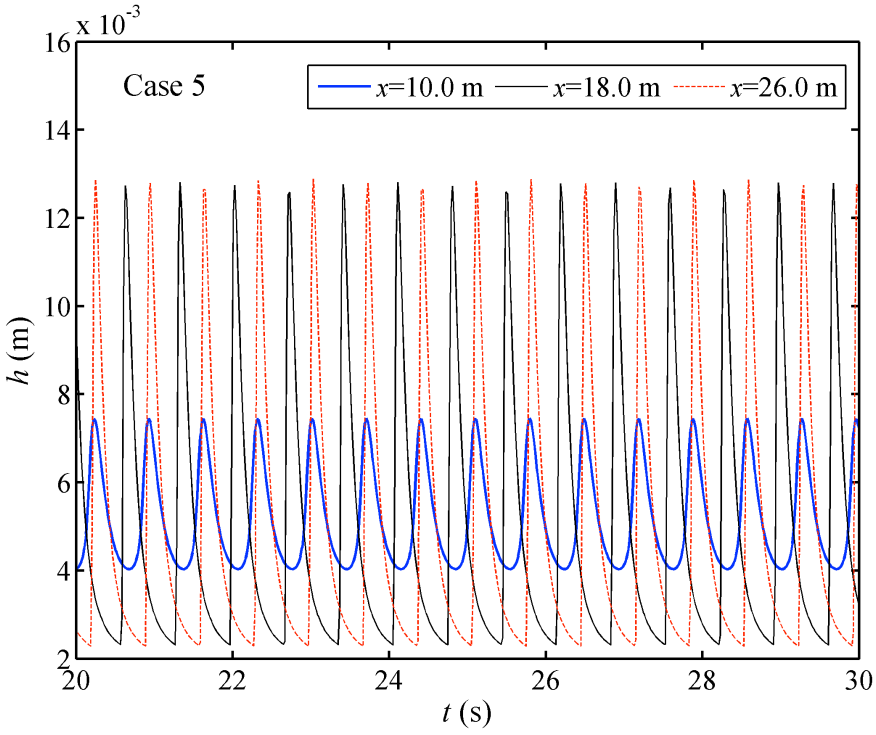

Figure 9 Computed water depths at different cross sections from the SWE-TM model

It takes a certain distance for perturbations to fully develop into periodic permanent roll waves (Brock 1967). The present computational tests show that larger perturbation amplitude imposed at the inlet is conducive to the formation of periodic permanent roll waves. Specifically, the distance required for perturbations to grow into periodic permanent roll waves decreases with the increase of the inlet perturbation amplitude, which echoes Brock's (1967) observation. If the dimensionless perturbation amplitude h_{am} / h_n imposed at the inlet of the channel is set to be 0.5%, 1.0%, 2.0% and 5.0% for Case 5, the formation distances of periodic permanent roll waves is equal to 16.3 m, 15.2 m, 14.0 m and 10.4 m respectively. This is illustrated in Fig. 10(a, b) for h_{am} / h_n=5.0% and 0.5%. However, the amplitude and period of the periodic permanent roll waves are independent of the perturbation amplitude at the inlet, which has not been revealed by Brock (1967). As shown in Fig. 11(a, b), the amplitude and period are always equal to 10.6 mm and 0.695 s respectively, irrespective of the inlet perturbation amplitude.

Further, the shorter the inlet perturbation period, the shorter the distance required for the formation of periodic permanent roll waves. This is shown in Table 2, and also illustrated in Fig. 10(b, c) for Cases 5 and 6. However, the period of periodic permanent roll waves is always equal to the inlet perturbation period imposed (0.695 s and 1.015 s respectively), as shown in Fig. 11(b, c). Further, the present computational tests show that the amplitude of periodic permanent roll waves increases with the increase of the inlet perturbation period, which has not been revealed by Brock (1967). When the inlet perturbation period is set to be 0.695 s (Case 5), 0.775 s, 0.855 s, 0.935 s and 1.015 s (Case 6) for the case with slope $\tan\theta$=0.1201, the amplitudes of the periodic permanent roll waves is respectively equal to 10.6 mm, 11.3 mm, 11.9 mm, 12.5 mm and 13.0 mm. This is shown in Fig. 11(b, c) for Case 5 and Case 6.

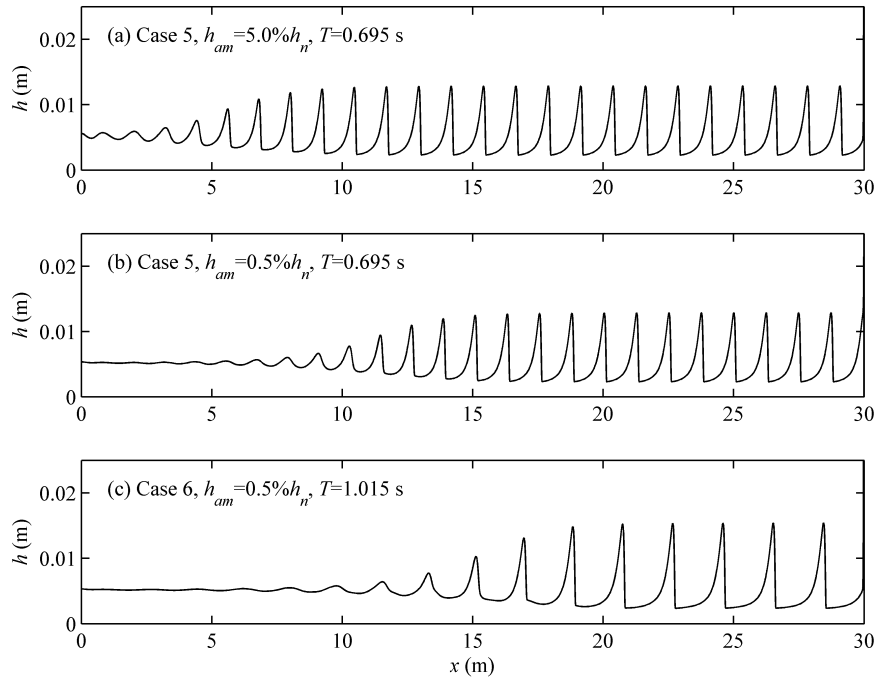

1

2 Figure 10 Computed water depths at t=80 s related to different inlet perturbation amplitudes and

3 periods

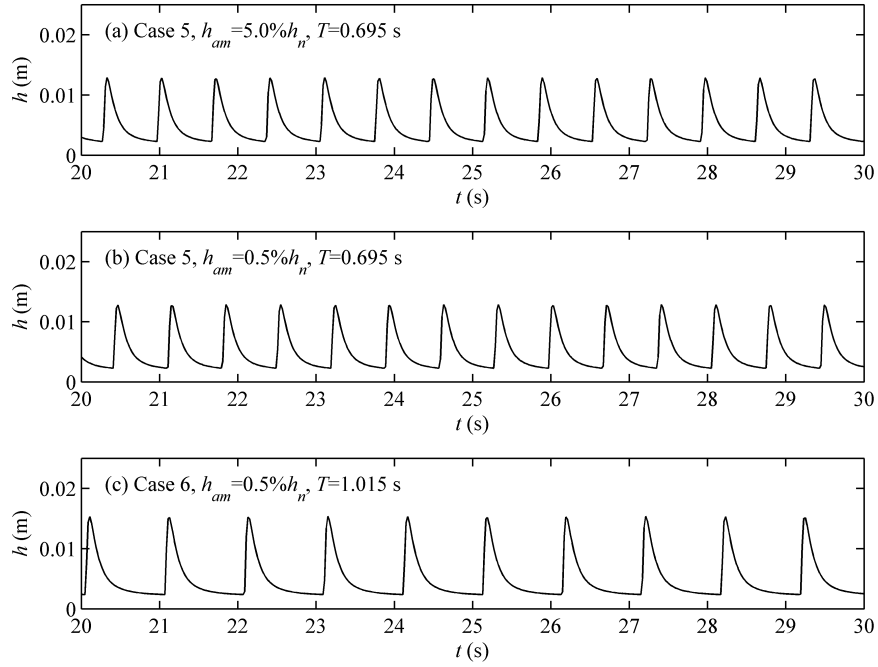

4

5 Figure 11 Computed water depths of periodic permanent roll waves at x=24.0 m related to different

inlet perturbation amplitudes and periods

4. Case study – natural roll waves

Roll waves are generally non-periodic and non-permanent in engineering practice due to the uncontrolled disturbances. Brock (1967) conducted a serious of experiments to investigate natural roll waves, in addition to periodic permanent roll waves. Zanuttigh and Lamberti (2002) numerically modelled the evolution of natural roll waves using traditional SWEs without considering the impacts of turbulence. However, their numerical study is open to question because their model was not verified by observed data, though detailed measured data is available for periodic permanent roll waves (Brock 1967). Likewise, the RGE model (Richard and Gavrilyuk 2012) cannot simulate the development of natural roll waves. This subsection aims to investigate natural roll waves by using the present SWE-TM model. In this regard, it is noted that Brock's experiments were constrained by the limited dimensions of the flumes. Thus for the computational study, the channel extends downstream to a length of 350 m to reveal the features of natural roll waves over a long distance. The downstream boundary conditions are set in a similar way as for the modelling of periodic permanent roll waves.

4.1 *Threshold period for natural roll waves*

For periodic permanent roll waves, the inlet paddle was oscillated at the desired period T (Brock 1967). In contrast, the perturbation conditions at the inlet were not described for natural roll waves in Brock (1967). The present computational tests reveal for the first time that a regular inlet perturbation may lead to either periodic permanent or natural roll waves, when its period is shorter or longer than a critical value T_c inherent to a specified normal flow. Apart from this, when the perturbation period is slightly shorter than T_c, instabilities and irregular waves may be spotted during the initial stage but periodic permanent roll waves ultimately generate after advancing a long distance. Physically, it is suggested herein that the shallow flow over a steep slope bear inherent waves with a frequency spectrum that is determined by the prescribed normal flow depth and velocity along with the bed slope and its roughness. Migrating downstream, the perturbations of sufficiently short periods imposed at the inlet of the channel are well accommodated by the inherent waves, and resonance occurs so that

the perturbations are enhanced, gradually grow and finally develop into periodic permanent roll waves. In contrast, the perturbations of long periods imposed at the inlet cannot be accommodated by the inherent waves of a specific frequency spectrum. In general, the perturbations are out of phase with the inherent waves. The interactions in between lead to irregular waves of disparate crests and troughs, and ultimately natural roll waves form. According to this mechanism, natural roll waves will form if an irregular, random perturbation is imposed at the inlet, i.e., Eq. (21), as demonstrated below.

The critical inlet perturbation period T_c from the present computational tests are summarized in Table 8. In fact, the basic conditions in Table 8 are the same as in Table 2, except the period and amplitude of the regular perturbations imposed at the inlet of the channel. Indeed, the critical period T_c is case specific, depending on the prescribed normal flow depth, velocity along with the bed slope and its roughness. It seems hard to formulate a relationship for the critical period T_c based on the limited number of cases with observed data (Table 8), for which further investigations are warranted.

In relation to Case 5 along with an inlet perturbation period T =3.0 s (longer than T_c), Figure 12 shows the computed water depths from the SWE-TM model at t =80.0 s. The free surface varies gently in the upstream region near the inlet of the channel until instabilities occur. These small instabilities magnify spontaneously as they propagate downstream, and finally evolve into natural roll waves. Figure 13 illustrates the computed water depth versus time from the SWE-TM model at cross sections x =30.0 m and 70.0 m. Minor visible instabilities are spotted at x =30.0 m, and these develop into large-amplitude natural roll waves as they propagate downstream. The wave front reaches the cross sections x =30.0 m and 70.0 m respectively at t =22.7 s and 52.5 s.

Table 8 Summary of natural roll waves cases

Case	$\tan\theta$	Q ($m^3 s^{-1}$)	h_n (mm)	F_n	C_f	T_c (s)	h_{am}/h_n
1	0.0502	9.72×10^{-4}	7.98	3.71	0.0032	4.69	0.5%
3	0.0846	6.52×10^{-4}	5.28	4.63	0.0036	2.12	0.5%
5	0.1201	8.02×10^{-4}	5.33	5.6	0.0035	2.20	0.5%

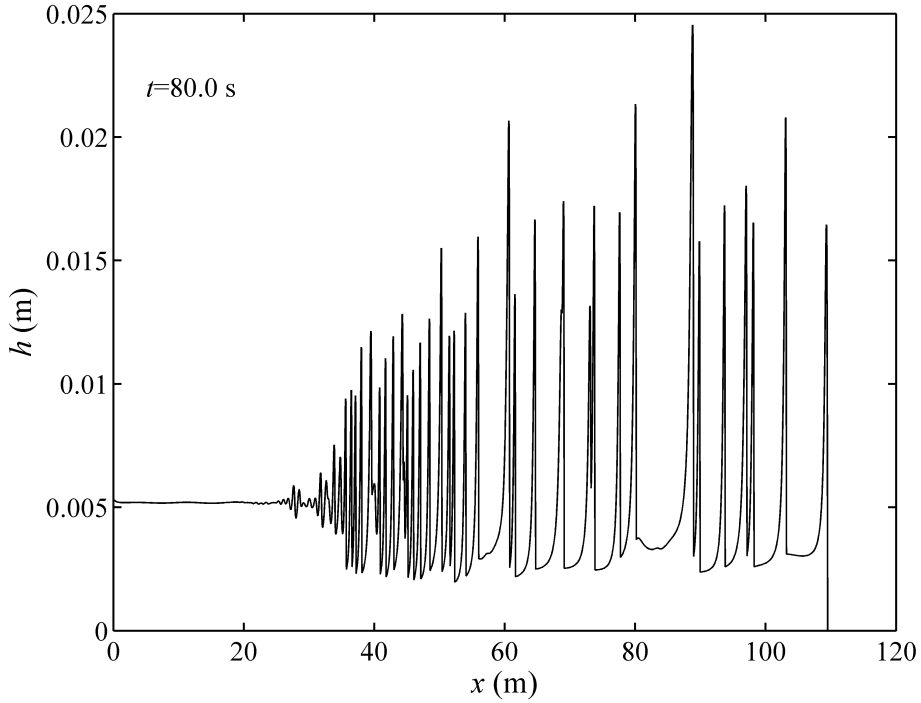

Figure 12 Computed water depths at t =80.0 s from the SWE-TM models with T =3.0 s

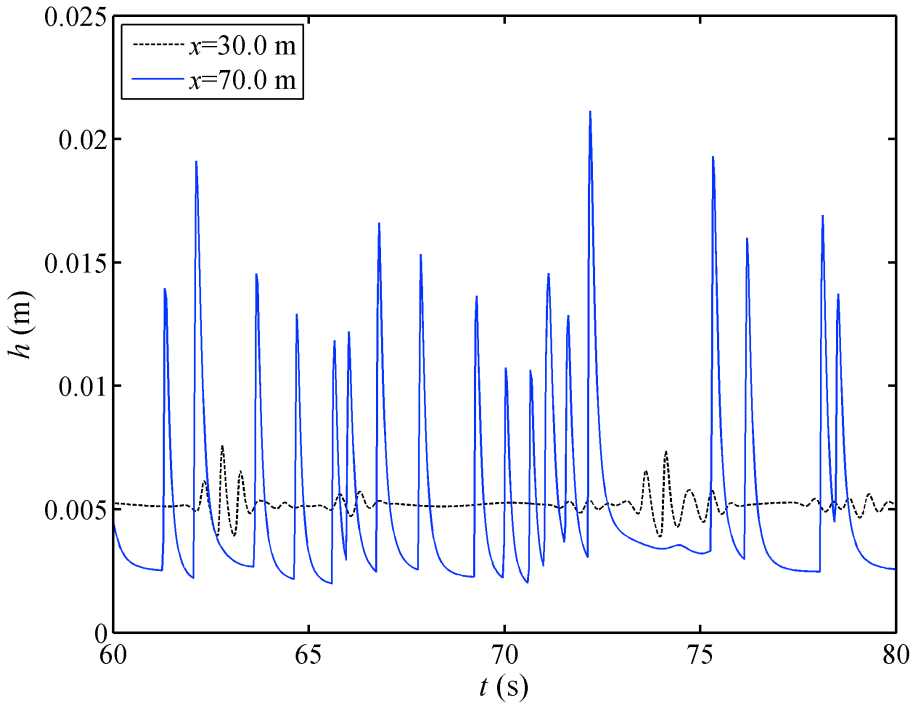

Figure 13 Computed water depths from the SWE-TM model, characterizing the formation of large-amplitude natural roll waves downstream from wavelets in the upstream

4.2 *Statistical properties of natural roll waves*

Natural roll waves were generated in flume experiments and their average properties were measured at several cross sections along the channel (Brock 1967). Here the SWE-TM model is deployed to resolve natural roll waves. As the inlet perturbation characteristics were not described for natural roll waves by Brock (1967), regular and irregular perturbations are respectively imposed at the inlet. A steady water discharge Q is fed at the inlet. The water depth in relation to a regular inlet perturbation is represented by Eq. (18), with a period longer than the critical period T_c (Table 8). The water depth related to an irregular perturbation is set as

$$h_{in} = h_n + h_{am} Random(-1,1) \tag{21}$$

where $Random(-1,1)$ is a function that generates random numbers between -1 to 1. Here Case 5 is considered to investigate the statistical properties of natural roll waves. The effects of the inlet perturbation characteristics are examined by computational tests as summarized in Table 9.

Table 9 Summary of computational tests for Case 5

Test	Perturbation characteristics	h_{am}/h_n	T_c
1	Regular	0.5%	3.5 s
2		5.0%	3.5 s
3	Irregular	0.5%	N/A
4		5.0%	N/A

Figures 14 to 16 show the computed dimensionless average wave properties $\bar{h}'_{max} = \bar{h}_{max}/h_n$, $\bar{h}'_{min} = \bar{h}_{min}/h_n$ and $\bar{T}' = \bar{T}\sin\theta\sqrt{g/h_n}$ in line with $l\sin\theta/h_n$ from the present SWE-TM model in relation to different inlet perturbation characteristics and the numerical solutions of Zanuttigh and Lamberti (2002), along with the measured data from Brock (1967). Here $\bar{h}_{\max}$, $\bar{h}_{\min}$ and $\bar{T}$ are respectively the average maximum depth, minimum depth and wave period, and l is the distance from the inlet along the channel. In calculating the average properties of natural roll waves, the duration for averaging is set to be 100 s, which is long enough so that any longer duration does not affect the results.

During the formation process of natural roll waves, the dimensionless average maximum depth $\overline{h}'_{max}$ and period $\overline{T}'$ increase and the dimensionless average minimum depth $\overline{h}'_{min}$ decreases, which are qualitatively consistent with Brock's (1967) observations. Also, the present computational tests demonstrate that natural roll waves may feature stable average properties (i.e., $\overline{h}'_{max}$ and $\overline{h}'_{min}$) after advancing a sufficiently long distance (Figs. 14 and 15), which was not revealed in Brock's (1967) experiments that were inevitably constrained by the limited dimensions of the flumes. In this regard, the present computations are preliminary, and further studies are warranted.

The present computational tests show that an irregular perturbation at the inlet is conducive to the formation of natural roll waves, as the distance from the inlet to the onset of detectable instabilities is considerably shorter than its counterpart with a regular perturbation of the same amplitude. Also, the larger the amplitude of the inlet perturbation, either regular or irregular, the shorter the distance required for the onset of discernible instabilities, which qualitatively agrees with Brock's (1967) observations.

Quantitatively, in the tests with regular inlet perturbations, the computed $\overline{h}'_{max}$ and $\overline{T}'$ start to increase and $\overline{h}'_{min}$ begins to decrease at a cross-section considerably downstream its counterpart in Brock's (1967) experiments. In the tests with irregular inlet perturbations (especially one of a larger amplitude) the statistical properties are closer to the measured data than those with regular inlet perturbations, yet the discrepancies between the computed results and observed data are still appreciable. Physically, this is because the inlet perturbation characteristics in Brock's (1967) experiments were not specified for use in the present computations, though these could significantly affect the formation of natural roll waves as stated by Brock (1967). Comparatively, the computed $\overline{h}'_{max}$ and $\overline{T}'$ from Zanuttigh and Lamberti (2002) seem to agree with observed data (Brock 1967) similarly well to those from the present SWE-TM model with irregular perturbations (Figs. 14 and 16), but $\overline{h}'_{min}$ from Zanuttigh and Lamberti (2002) deviates significantly from the measured data (Fig. 15), especially its mean growth rate along the channel. The fact that turbulence is totally ignored in Zanuttigh and Lamberti (2002), in addition to the difference in inlet perturbation characteristics, may have led to the disparate results compared to those of the present SWE-TM model.

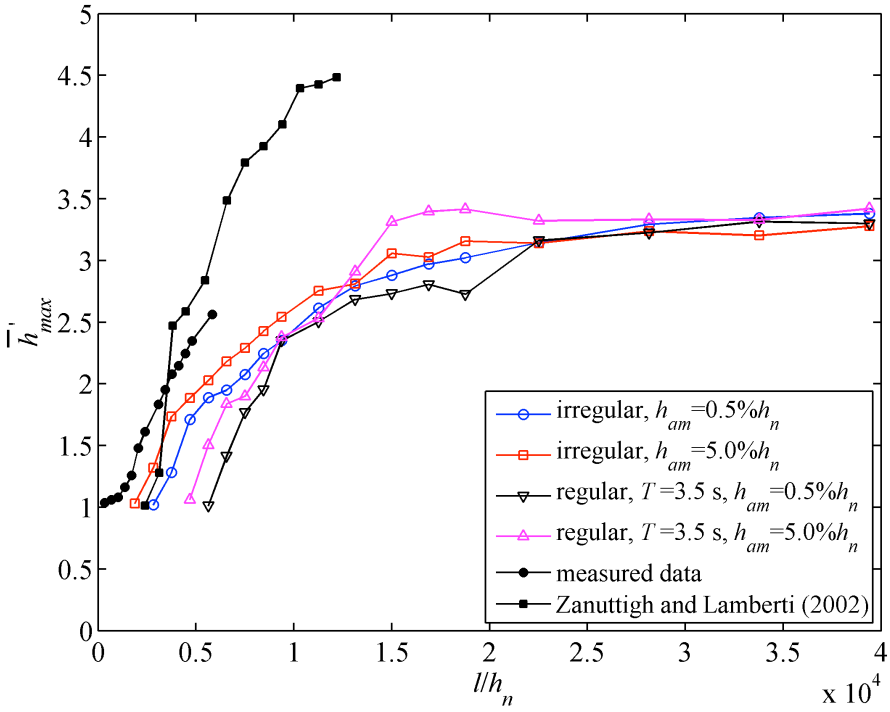

Figure 14 Comparison of $\bar{h}'_{max}$ from numerical results and measured data from Brock (1967)

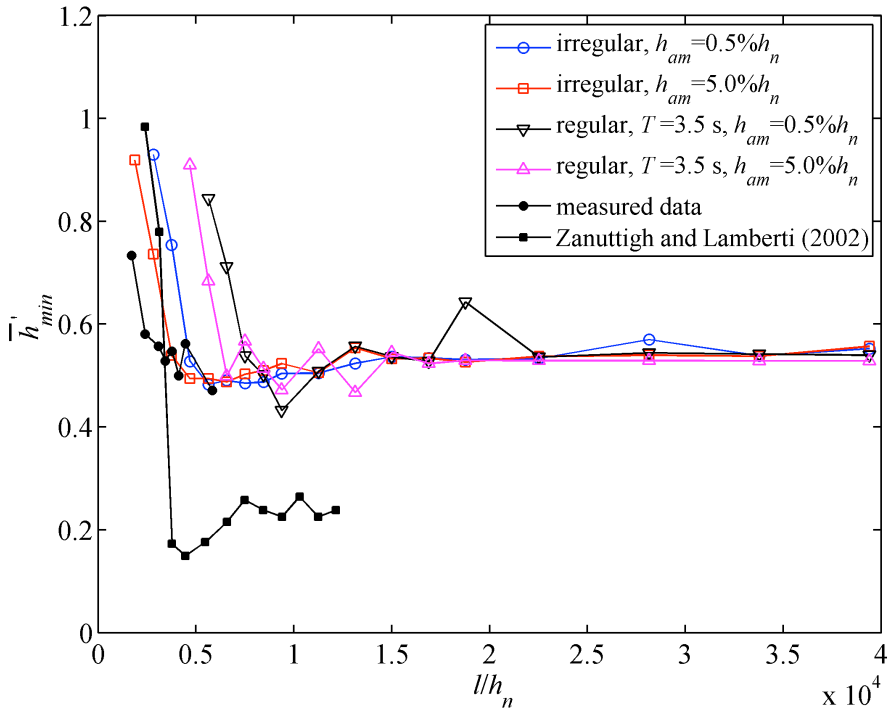

Figure 15 Comparison of $\bar{h}'_{min}$ from numerical results and measured data from Brock (1967)

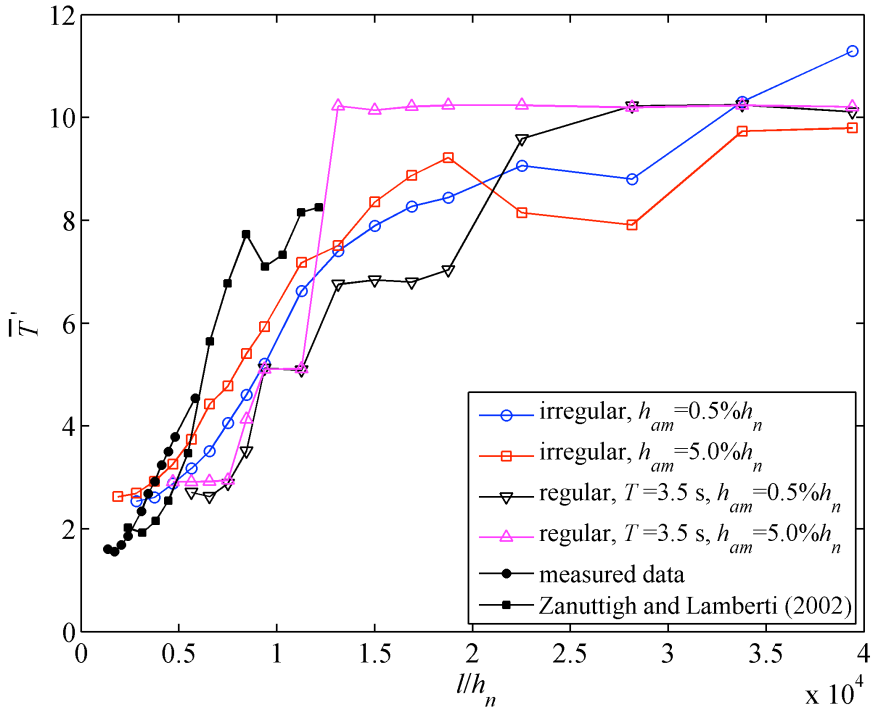

Figure 16 Comparison of $\bar{T}'$ from numerical results and measured data from Brock (1967)

The scaling l/h_n in Figs. 14-16 was proposed by Brock (1967). Apart from this scaling, in response to the comments by Montuori (2005), Zanuttigh and Lamberti suggested that the dimensionless average wave properties versus $l\sin\theta/h_n$ could be unified for different bed slopes. This is examined here as per Cases 1, 3 and 5. Shown in Figs. 17-19 are $\bar{h}'_{max}$, $\bar{h}'_{min}$ and $\bar{T}'$ from the SWE-TM model with irregular inlet perturbations of amplitude $h_{am}=5.0\%h_n$ and also Zanuttigh and Lamberti (2002), along with the measured data from Brock (1967). It is seen from Figs. 17-19 that the average wave properties are roughly unified during the early growth stage of the natural roll waves (i.e., well before the maximum and minimum depths become stable). However, in the long term when the observed data from Brock (1967) did not cover, the dimensionless average maximum and minimum depths and period segregate from each other for different bed slopes. This holds for the numerical results from either the present SWE-TM model or Zanuttigh and Lamberti (2002). Therefore, the dimensionless average properties of natural roll waves are dictated by more complex mechanisms in addition to the impact of the bed slope, which merits further investigation.

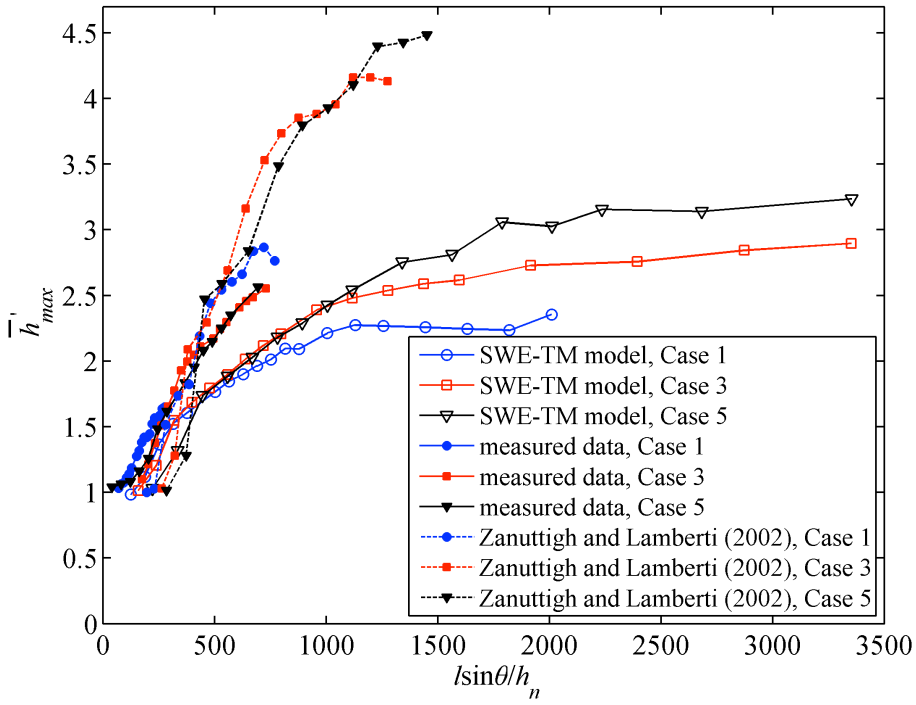

Figure 17 Comparison of $\bar{h}'_{max}$ from numerical results and measured data from Brock (1967) for different bed slopes

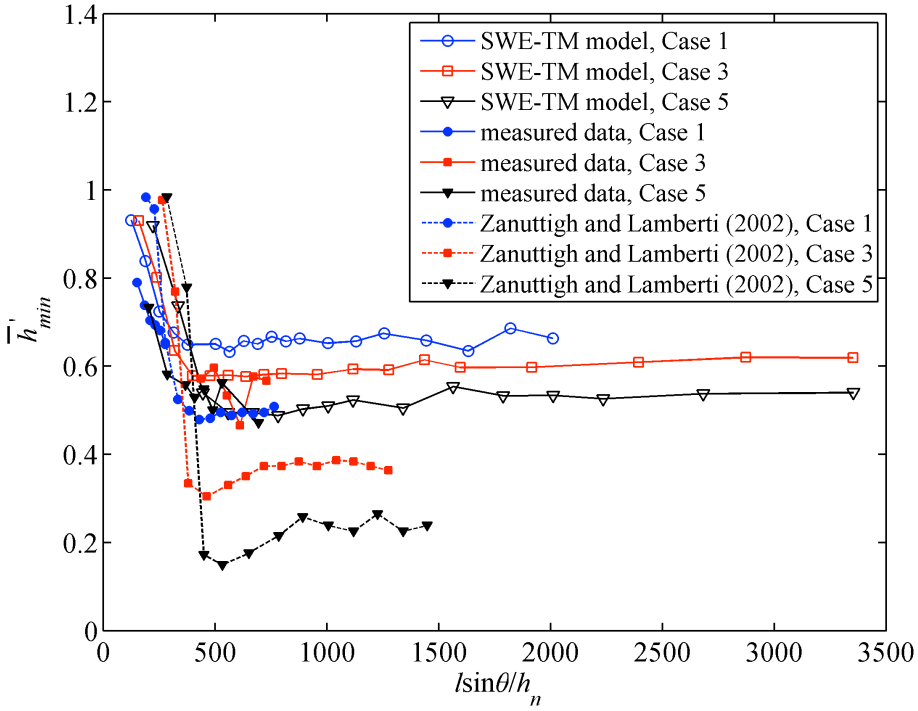

Figure 18 Comparison of $\bar{h}'_{min}$ from numerical results and measured data from Brock (1967) for different bed slopes

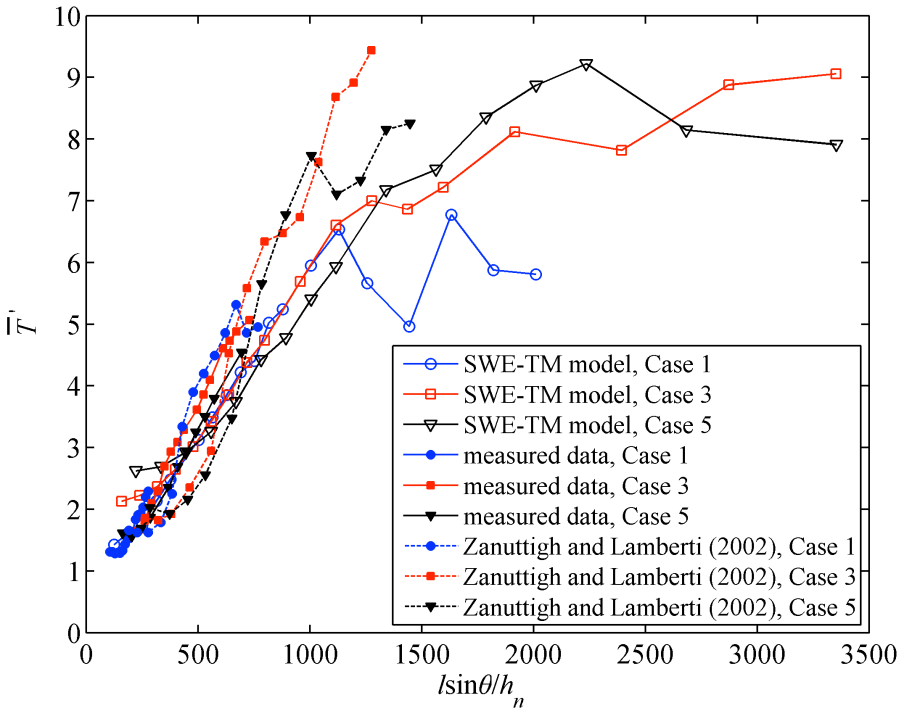

Figure 19 Comparison of $\bar{T}'$ from numerical results and measured data from Brock (1967) for different bed slopes

5. Conclusions

A physically enhanced shallow water hydrodynamic model, SWE-TM, is proposed for roll waves, which explicitly incorporates turbulent Reynolds stress based on the standard depth-averaged $k-\varepsilon$ model along with a modification component. The present model is applied to investigate both periodic permanent and natural roll waves. The following conclusions are drawn.

- The SWE-TM model features improved performance over the SWE, SWE-T, SWE-TD and RGE models, as compared with measured data on periodic permanent roll waves (Brock 1967). This clearly certifies the significance of turbulent Reynolds stress for roll waves modelling. The SWE-TM model can be used to simulate not only the final pattern of periodic permanent roll waves, but also the formation processes of periodic permanent and natural roll waves, which cannot be resolved by the RGE model (Richard and Gavrilyuk 2012). More systematic observations of roll waves are warranted to further modify the present SWE-TM model, which

should facilitate physically enhanced modelling of complex flows over steep slopes.

- A regular inlet perturbation may lead to periodic permanent (Figs. 8-11) or natural roll waves (Figs. 12-15), when its period is shorter or longer than a critical value inherent to a specified normal flow. An irregular, random inlet perturbation favours the formation of natural roll waves (Figs. 14 and 15).
- A larger amplitude or shorter period of the inlet perturbation is conducive to the formation of periodic permanent roll waves (Fig. 10), which concurs with Brock's (1967) observation. The amplitude of periodic permanent roll waves is independent of the perturbation amplitude at the inlet but increases with the increase of inlet perturbation period (Figs. 10 and 11), while the period is the same as that of the inlet perturbation (Fig. 9).
- A larger amplitude of the inlet perturbation is conducive to the formation of natural roll waves (Figs. 14 and 15), which is consistent with Brock's (1967) observations. During the formation process of natural roll waves, the average maximum depth and period increase whereas the average minimum depth decreases (Figs. 14-16). Natural roll waves may feature stable average maximum and minimum depths after advancing a sufficiently long distance (Figs. 14 and 15).

Acknowledgement

The research is funded by Natural Science Foundation of China [Grant No. 51279144], [Grant no. 11432015] on debris floods and also Chinese Academy of Sciences [Grant No. KZZD-EW- 05-01-03] on debris flow and its interaction with engineering structures.

Notations

C = coefficient in Eq. (15) (-)

C_f = bed friction coefficient (-)

Cr = Courant number (-)

C_μ, $C_{\varepsilon 1}$, $C_{\varepsilon 2}$, C_Γ = coefficients of the $k-\varepsilon$ model (-)

D = dispersion momentum transport ($m^3\ s^{-2}$)

$\boldsymbol{F}$ = vector defined in Eq. (11)

F = Froude number (-)

F_n = Froude number refers to the normal conditions at the inlet (-)

g = gravitational acceleration ($m\ s^{-2}$)

$g' = g\cos\theta$ ($m\ s^{-2}$)

h = water depth in the normal direction of slope (m)

h_{am} = perturbation amplitude imposed at the inlet of the channel (m)

$\overline{h}_{max}$ = average maximum water depth (m)

$\overline{h}_{min}$ = average minimum water depth (m)

h_n = normal depth (m)

h_{in} = water depth at the inlet of the channel (m)

h^* = dimensionless water depth (-)

$\hat{h}$ = dimensionless measured data (-)

$\overline{h}'_{max}$ = dimensionless average maximum water depth (-)

$\overline{h}'_{min}$ = dimensionless average minimum water depth (-)

i = index denoting the spatial node

j = index denoting the time step

k = depth-averaged turbulent kinetic energy ($m^2\ s^{-2}$)

L^1 = norm to measure error (-)

l = distance along channel from the inlet to a cross section (m)

l_p = formation distance from the inlet to the appearance of periodic permanent roll waves (m)

m = coefficient in Eq. (5a) (-)

P_k = production term due to the horizontal velocity gradients in Eqs. (7) and (8) ($m^2 s^{-3}$)

P_{kb} = production term due to bed friction effect in Eq. (7) ($m^2 s^{-3}$)

$P_{\varepsilon b}$ = production term due to bed friction effect in Eq. (8) ($m^2 s^{-4}$)

p = index denoting the state after calculating variables from Eq. (13)

Q = upstream discharge ($m^3 s^{-1}$)

q = conservative variable in Eq. (12a) ($m^2 s^{-1}$)

Re = Reynolds number (-)

r = hydraulic radius (m)

$\boldsymbol{S}$ = vector defined in Eq. (11)

$\boldsymbol{S}_s$, $\boldsymbol{S}_f$, $\boldsymbol{S}_d$ = source terms defined in Eq. (12c) ($m^2 s^{-2}$)

S_D, S_G, S_{T_R} = dispersion term, gravity term and turbulent Reynolds stress term in Eq. (2) ($m^2 s^{-2}$)

T = wave period (s)

$\overline{T}$ = average wave period (s)

$\overline{T}'$ = dimensionless average wave period (-)

T_0 = Reynolds stress closed by the standard $k-\varepsilon$ model ($m^2 s^{-2}$)

T_a = Reynolds stress closed by the standard $k-\varepsilon$ model with a modification ($m^2 s^{-2}$)

T_c = critical perturbation period (s)

T_R = depth-averaged Reynolds stress ($m^2 s^{-2}$)

t = time (s)

$\boldsymbol{U}$ = vector defined in Eq. (11)

U = depth-averaged streamwise velocity ($m s^{-1}$)

u_* = friction velocity ($m s^{-1}$)

$\overline{u}(z)$ = the streamwise velocity distribution in vertical ($m s^{-1}$)

x = streamwise coordinate (m)

z = vertical coordinate (m)

z_0 = zero velocity level (m)

Greek

Δx = spatial step in the x direction (m)

Δt = time step (s)

α = coefficient to be calibrated in Eq. (9) (-)

β = momentum flux correction (-)

β_{power} = momentum flux correction based on power law distribution (-)

β_{log} = momentum flux correction based on log law distribution (-)

ε = depth-averaged diffusion rate of turbulent kinetic energy ($m^2 s^{-3}$)

φ = a small-scale enstrophy defined by Richard and Gavrilyuk (s^{-2})

Φ = a large-scale enstrophy defined by Richard and Gavrilyuk (s^{-2})

ϕ = variables in Eq. (15) (-)

η_0 = dimensionless zero bed elevation (m) (-)

θ = angle of bottom slope (rad)

λ = wave length (m)

ν = kinematic viscosity of water ($m^2 s^{-1}$)

ν_t = depth-averaged eddy viscosity ($m^2 s^{-1}$)

ρ = density of water ($kg\ m^{-3}$)

σ_k, σ_ε = coefficients of the $k-\varepsilon$ model (-)

τ_b = bed shear stress ($kg\ m^{-1} s^{-2}$).

References

Balmforth, N.J., Mander, S. (2004). Dynamics of roll waves. *J. Fluid Mech*. 514, 1-33.

Benjamin, T.B. (1957). Wave formation in laminar flow down an inclined plane. *J. Fluid Mech*. 2, 554-574.

Bouchut, F., Mangeney-Castelnau, A., Perthame, B., Vilotte, J. P. (2003). A new model of Saint Venant and Savage–Hutter type for gravity driven shallow water flows. *C. R. Acad. Sci. Paris, Ser. I* 336(6), 531-536.

Brock, R.R. (1967). Development of roll waves in open channels. *PhD thesis*, W. M. Keck Laboratory of Hydraulics and Water Resources, California Institute of Technology, USA.

Brock, R.R. (1970). Periodic permanent roll-waves. *J. Hydraulic Div.* 96(12), 2565-2580.

Cao, Z.X., Pender, G., Wallis, S., Carling, P. (2004). Computational dam-break hydraulics over erodible sediment bed. *J. Hydraulic Eng.* 130(7), 689-703.

Cornish, V. (1934). *Ocean waves and kindred geophysical phenomena*. Cambridge University Press, Cambridge.

Dressler, R.F. (1949). Mathematical solution of the problem of roll-waves in inclined open channels. *Comm. on Pure and Appl. Math*. 2, 149-194.

Dressler, R.F., Pohle, F.V. (1953). Resistance effects on hydraulic instability. *Comm. on Pure and Appl. Math.* 6(1), 93-96.

Duan, J.G., Nanda, S.K. (2006). Two-dimensional depth-averaged model simulation of suspended sediment concentration distribution in a groyne field. *J. Hydrology* 327(3), 426-437.

Gharangik, A.M., Chaudhry, M.H. (1991). Numerical simulation of hydraulic jump. *J. Hydraulic Eng.* 117(9), 1195-1211.

Iwasa, Y. (1954). The criterion for instability of steady uniform flows in open channels. Memoirs of the Faculty of Engineering, Kyoto University, Japan, 16(6), 264-275.

Iverson, R.M., Logan, M., LaHusen, R.G., Berti, M. (2010). The perfect debris flow? Aggregated

results from 28 large-scale experiments. *J. Geophys. Res.* 115, F03005.

Jeffreys, H.J. (1925). The flow of water in an inclined channel of rectangular section. *Phil. Magazine* 6(49), 793-807.

Jin, Y.C., Steffler, P.M. (1993). Predicting flow in curved open channels by depth-averaged method. *J. Hydraulic Eng.* 119(1), 109-124.

Kranenburg, C. (1992). On the evolution of roll waves. *J. Fluid Mech.* 245(1), 249-261.

Launder, B.E., Spalding, D.B. (1974). The numerical computation of turbulent flows. *Comp. Meth. In Appl. Mech. Eng*. 3, 26-289.

Li, J., Cao, Z.X., Pender, G., Liu, Q.Q. (2013). A double layer-averaged model for dam-break flows over erodible bed. *J. Hydraulic Res.* 51(5), 518-534.

Liu, K.F., Mei, C.C. (1994). Roll waves on a layer of a muddy fluid flowing down a gentle slope-A Bingham model. *Phys. Fluids* 6, 2577.

Liu, Q.Q., Chen, L., Li, J.C., Singh, V.P. (2005). Roll waves in overland flow. *J. Hydrologic Eng.* 10(2), 110-117.

Misra, S.K., Kirby, J.T., Brocchini, M.,Veron, F., Thomas, M., Kambhamettu, C. (2008). The mean and turbulent flow structure of a weak hydraulic jump. *Phys. Fluids* 20, 035106.

Montuori, C. (2005). Roll waves simulation using shallow water equations and weighted average flux method, *J. Hydraulic Res.* 43(1), 103-106.

Needham, D.J., Merkin, J.H. (1984). On roll waves down an open inclined channel. *Proc. R. Soc. Lond.* A 394, 259-278.

Ni, H.Q. (2010). *Turbulence simulation and application in modern hydraulics engineering*. China Water Power Press, Beijing (in Chinese).

Rastogi, A.K., Rodi, W. (1978). Predictions of heat and mass transfer in open channels. *J. Hydraulic Div.* 104(3), 397–420.

Richard, G.L., Gavrilyuk, S.L. (2012). A new model of roll waves: comparison with Brock's

1 experiments. *J. Fluid Mech.* 698, 374-405.

2 Rodi, W. (1993). *Turbulence models and their applications in Hydraulics.* IAHR Monograph,
3 Rotterdam.

4 Savage, S.B., Hutter, K. (1991). The dynamics of avalanches of granular materials from initiation to
5 run-out. Part I: Analysis. *Acta Mech*. 86(1-4), 201–223.

6 Shi, X.G. (1994). *Turbulent flow*. Tianjin University Press, Tianjin (in Chinese).

7 Stoker, J.J. (1958) *Water waves, the mathematical theory with applications.* John Wiley & Sons, New
8 York.

9 Tamburrino, A., Ihle, C.F. (2013). Roll wave appearance in bentonite suspensions flowing down
10 inclined planes. *J. Hydraulic Res.* 51(3), 330-335.

11 Toro, E.F. (2001). *Shock-capturing methods for free-surface shallow flows.* John Wiley & Sons,
12 Chichester.

13 Wu, W. (2007). *Computational river dynamics*. Taylor & Francis, London, UK.

14 Yih, C. (1963). Stability of liquid flow down an inclined plane. *Phys. Fluids*. 6(3), 321-334.

15 Yu, J., Kevorkian, J. (1992). Nonlinear evolution of small disturbances into roll waves in an inclined
16 open channel. *J. Fluid Mech.* 243, 575-575.

17 Zanuttigh, B., Lamberti, A. (2002). Roll waves simulation using shallow water equations and
18 weighted average flux method. *J. Hydraulic Res.* 40(5), 610-622.

19 Zanuttigh, B., Lamberti, A. (2007). Instability and surge development in debris flows. *Rev. Geophys.*
20 45(3), RG3006.

21

22

List of tables

List of figure captions

Figure 1 Comparison between the computed water depth from the SWE, SWE-T and SWE-TD models and measured data from Brock (1967)

Figure 2 Comparison between the computed water depth from the SWE-TM model using calibrated α and measured data from Brock (1967)

Figure 3 Comparison between the computed water depth from SWE-TM model using tuned C_Γ for Case 1 and measured data from Brock (1967)

Figure 4 Comparison between the computed water depth and measured data from Brock (1967)

Figure 5 Computed Reynolds stress compared to the gravitational terms in a single permanent roll wave from the SWE-TM model

Figure 6 Impacts of α on water depth in SWE-TM model

Figure 7 Impacts of C_Γ on water depth in SWE-TM model

Figure 8 Formation process of periodic permanent roll waves in Case 5

Figure 9 Computed water depths at different cross sections from the SWE-TM model

Figure 10 Computed water depths at t =80 s related to different inlet perturbation amplitudes and periods

Figure 11 Computed water depths of periodic permanent roll waves at x=24.0 m related to different inlet perturbation amplitudes and periods

Figure 12 Computed water depths at t=80.0 s from the SWE-TM models with T=3.0 s

Figure 13 Computed water depths from the SWE-TM model, characterizing the formation of large-amplitude natural roll waves downstream from wavelets in the upstream

Figure 14 Comparison of $\overline{h}'_{max}$ from numerical results and measured data from Brock (1967)

Figure 15 Comparison of $\overline{h}'_{min}$ from numerical results and measured data from Brock (1967)

Figure 16 Comparison of $\overline{T}'$ from numerical results and measured data from Brock (1967)

Figure 17 Comparison of $\overline{h}'_{\max}$ from numerical results and measured data from Brock (1967) for different bed slopes

Figure 18 Comparison of $\overline{h}'_{\min}$ from numerical results and measured data from Brock (1967) for different bed slopes

Figure 19 Comparison of $\overline{T}'$ from numerical results and measured data from Brock (1967) for different bed slopes